MBoC | BRIEF REPORT

The C-terminus of α-Synuclein Regulates its Dynamic Cellular Internalization by Neurexin 1β

Melissa Birol[a,b,*], Isabella Ioana Douzoglou Muñoz[b], and Elizabeth Rhoades[a,*]
[a]Department of Chemistry, University of Pennsylvania, Philadelphia, PA 19104; [b]Max Delbrück Institute for Molecular Medicine, Berlin Institute for Medical Systems Biology, Berlin 10115, Germany

ABSTRACT **The aggregation of the disordered neuronal protein, α-Synuclein (αS), is the primary pathological feature of Parkinson's disease. Current hypotheses favor cell-to-cell spread of αS species as underlying disease progression, driving interest in identifying the molecular species and cellular processes involved in cellular internalization of αS. Prior work from our lab identified the chemically specific interaction between αS and the presynaptic adhesion protein neurexin-1β (N1β) to be capable of driving cellular internalization of both monomer and aggregated forms of αS. Here we explore the physical basis of N1β-driven internalization of αS. Specifically, we show that spontaneous internalization of αS by SH-SY5Y and HEK293 cells expressing N1β requires essentially all of the membrane-binding domain of αS; αS constructs truncated beyond residue 90 bind to N1β in the plasma membrane of HEK cells, but are not internalized. Interestingly, before internalization, αS and N1β codiffuse rapidly in the plasma membrane. αS constructs that are not internalized show very slow mobility themselves, as well as slow N1β diffusion. Finally, we find that truncated αS is capable of blocking internalization of full-length αS. Our results draw attention to the potential therapeutic value of blocking αS–N1β interactions.**

Monitoring Editor
Jennifer Lippincott-Schwartz
Howard Hughes Medical Institute

Received: Nov 2, 2022
Revised: Jul 17, 2023
Accepted: Sep 15, 2023

INTRODUCTION

Alpha-synuclein (αS) is a small (140 residues), intrinsically disordered neuronal protein (Davidson *et al.*, 1998; Theillet *et al.*, 2016). In Parkinson's disease, αS is the primary component of intracellular fibrillar aggregates that are the hallmark of disease (Spillantini *et al.*, 1998; Galvin *et al.*, 1999). Natively, αS is primarily localized to presynaptic termini (Maroteaux *et al.*, 1988; Kahle *et al.*, 2000), where it binds reversibly to cellular membranes (Kahle *et al.*, 2000; Bussell and Eliezer, 2003; Fortin *et al.*, 2004; Bendor *et al.*, 2013). Because of its central role in Parkinson's disease and other synucleinopathies, αS is of major biomedical interest.

αS has three domains (Figure 1): 1) the first ~90 residues consist of seven, 11 residue imperfect repeats of a KTKEGV motif that mediate membrane binding through formation of a long, amphipathic helix (Bussell and Eliezer, 2003; Jao *et al.*, 2004; Ferreon *et al.*, 2009; Trexler and Rhoades, 2009); all six (A30P, E46K, H50Q, G51D, and A53T/E) mutations linked to familial forms of Parkinson's disease are found in this region; 2) the central non-amyloid component (NAC) domain between residues 61 and 95 that also makes up the core of aggregated synuclein fibers (Tuttle *et al.*, 2016; Guerrero-Ferreira *et al.*, 2018; Li *et al.*, 2018) is encompassed within the membrane-binding domain; and 3) the highly acidic C-terminus. Like many intrinsically disordered proteins, αS is subject to numerous posttranslational modifications, several of which are of interest as biomarkers or for putative roles in αS aggregation in disease (Beyer, 2006; Beyer and Ariza, 2013; Kellie *et al.*, 2014). While the majority of identified modifications to αS are found on only a fraction of the total protein (Kellie *et al.*, 2014), N-terminal acetylation has been identified on virtually all αS derived from human or other mammalian cells and tissue (Anderson *et al.*, 2006) and thus αS bearing this modification represents the physiological form of the protein.

While αS is primarily cytoplasmic, it is also found extracellularly and in cerebrospinal fluid (Lee *et al.*, 2005; Kang *et al.*, 2016; Bieri *et al.*, 2018; van Steenoven *et al.*, 2018; Zambon *et al.*, 2019). In Parkinson's disease, it has been proposed that propagation of pathological aggregates occurs via a prion-like mechanism, where toxic αS assemblies are released into the extracellular matrix by

This article was published online ahead of print in MBoC in Press (http://www.molbiolcell.org/cgi/doi/10.1091/mbc.E22-11-0496) on September 20, 2023.

*Address correspondence to: Melissa Birol (Melissa.Birol@mdc-berlin.de); Elizabeth Rhoades (elizabeth.rhoades@sas.upenn.edu).

Abbreviations used: N1β, neurexin 1β; αS, α-Synuclein; AL594, Alexa Fluor 594 C_5 maleimide; AL647, Alexa Fluor 647 C_5 maleimide; acetyl, N-terminally acetylated

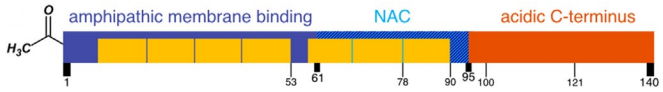

FIGURE 1: Schematic of αS_{acetyl}. Three major domains are labeled on the schematic and the seven, 11 residue membrane binding repeats are shown in yellow. Also marked are the truncations created for this study. For all constructs, a S9C mutation was made to allow for site-specific labeling.

"infected" neurons (Guo and Lee, 2014). These species are internalized by neighboring neurons, seeding aggregation of the endogenous αS in these cells. Although it lacks a canonical secretion sequence, cell culture models show that monomeric αS is continuously secreted to the extracellular media (Emmanouilidou *et al.*, 2010; Yamada and Iwatsubo, 2018) where it may be reinternalized. Consequently, there is significant interest in identifying and characterizing the molecular components and cellular pathways involved in the internalization of αS. A number of plasma membrane proteins have been identified as αS receptors (Shrivastava *et al.*, 2015; Mao *et al.*, 2016; Urrea *et al.*, 2017; Birol *et al.*, 2019; Diaz-Ortiz *et al.*, 2022). Prior work from our lab demonstrated that expression of the neuronal adhesion protein, neurexin-1β (N1β), in HEK293 cells is sufficient to cause spontaneous internalization of both monomer and fibrillar αS (Birol *et al.*, 2019). Moreover, this uptake showed chemical selectivity in that it was dependent both upon the N-terminal acetylation of αS as well as the N-linked glycan on the globular extracellular domain of N1β (Birol *et al.*, 2019).

As noted above, various neuronal cell surface receptors have been identified for different forms of αS – monomer, oligomer, and fibrillar – pointing to the existence of multiple internalization pathways. There is also evidence that the inhibition of any single endocytosis pathway is not sufficient to completely stop cellular entry of αS. Our current understanding of the molecular elements governing the internalization of αS is limited. Here we investigate the molecular features associated with N1β-driven internalization of αS_{acetyl}. Specifically, we used truncated variants of αS_{acetyl} to identify regions involved in N1β-mediated binding and uptake in HEK 293 cells. We show that full-length and truncated αS_{acetyl} bind comparably to HEK-N1β; however, they are not internalized to a similar degree. Specifically, we identify that the entire membrane-binding domain of αS_{acetyl} is essential for N1β-mediated internalization of αS_{acetyl}. Moreover, we measured the mobility of αS_{acetyl}/N1β complexes in the plasma membrane, before internalization, and found a correlation between the degree of mobility and the extent of uptake. Lastly, we report on a specific αS truncation that inhibits N1β-mediated internalization of full-length protein, opening a new avenue for therapeutic intervention focused on limiting the extracellular propagation of αS_{acetyl}.

RESULTS AND DISCUSSION

Robust spontaneous internalization of αS_{acetyl} requires the entire membrane-binding domain

Full-length N-terminally acetylated αS ($^{1–140}\alpha S_{acetyl}$) was obtained by coexpression of αS with the NatB complex from *Saccharomyces cerevisiae* in *Escherichia coli* (Johnson *et al.*, 2010; Trexler and Rhoades, 2012; Birol *et al.*, 2019). Truncated constructs of αS were created by introduction of a stop codon at the appropriate location in the plasmid encoding full-length αS. $^{1–121}\alpha S_{acetyl}$ and $^{1–100}\alpha S_{acetyl}$ were chosen because truncations near these residues have been identified in human tissue (Anderson *et al.*, 2006; Kellie *et al.*, 2014; Bhattacharjee *et al.*, 2019); $^{1–90}\alpha S_{acetyl}$, $^{1–78}\alpha S_{acetyl}$, and $^{1–53}\alpha S_{acetyl}$ were selected because they correspond to fragments spanning seven, six, and four of the membrane binding repeats, respectively (Figure 1). A serine to cysteine mutation was made at residue nine to allow for site-specific labeling with Alexa 594 (AL594) maleimide. We have fluorescently labeled αS at this position with several different fluorophores and found minimal impact on its properties in a number of studies (Trexler and Rhoades, 2009, 2010; Middleton and Rhoades, 2010; Sevcsik *et al.*, 2011; Nath *et al.*, 2012).

SH-SY5Y is a neuroblastoma-derived immortal cell line that is frequently used as a model system for studies involving αS because these cells maintain many of the pathways that are dysregulated in Parkinson's disease (Krishna *et al.*, 2014). Moreover, they spontaneously internalize both monomer and preformed fibrillar (PFF) αS (Rodriguez *et al.*, 2018; Birol *et al.*, 2019). SH-SY5Y cells were incubated with 200 nM AL594 αS_{acetyl}. Following 12-h incubation, the media were exchanged to remove any remaining αS_{acetyl} and the cells were imaged. Internalized αS_{acetyl} can be seen as punctate structures in the cell body (Figure 2A), which we know from our prior work to be acidic endosomes or lysosomes (Birol *et al.*, 2019). Comparable levels of uptake were found in cells incubated for 12 h with $^{1–140}\alpha S_{acetyl}$, $^{1–121}\alpha S_{acetyl}$, and $^{1–100}\alpha S_{acetyl}$, while cells incubated with $^{1–78}\alpha S_{acetyl}$ and $^{1–53}\alpha S_{acetyl}$ did not show significant internalization (Figure 2, A and B).

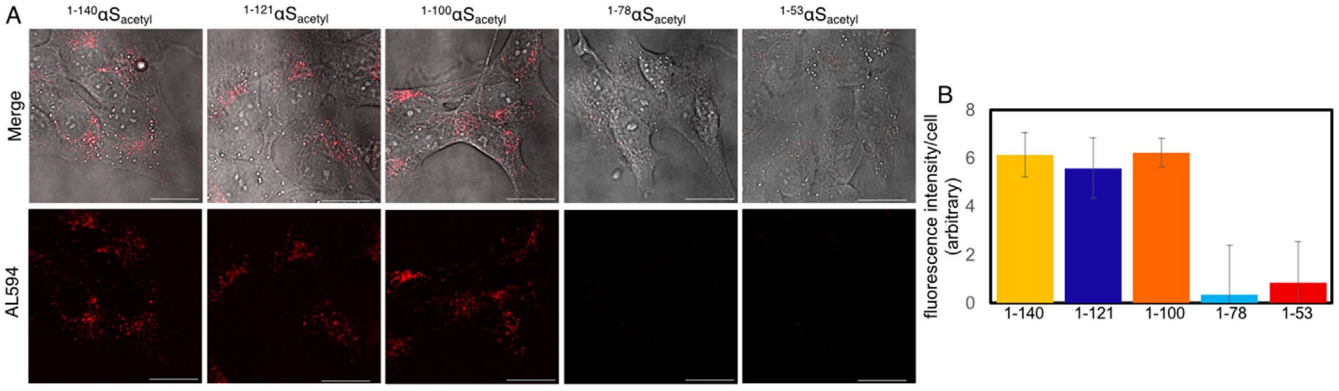

FIGURE 2: Internalization in SH-SY5Y is reduced for truncated αS_{acetyl} constructs. (A) Representative images of SH-SY5Y cells following 12-h incubation with AL594 αS_{acetyl} variants. The fluorescence images are shown with (upper) and without (lower) differntial interference contrast merge. (B) Quantification of extent of spontaneous internalization of αS_{acetyl} constructs by SH-SY5Y cells. Images obtained after 12-h incubation with protein and quantified by total fluorescence intensity per cell. Analysis based on $n = 100$ cells, three independent experiments. Scale bars = 20 μm.

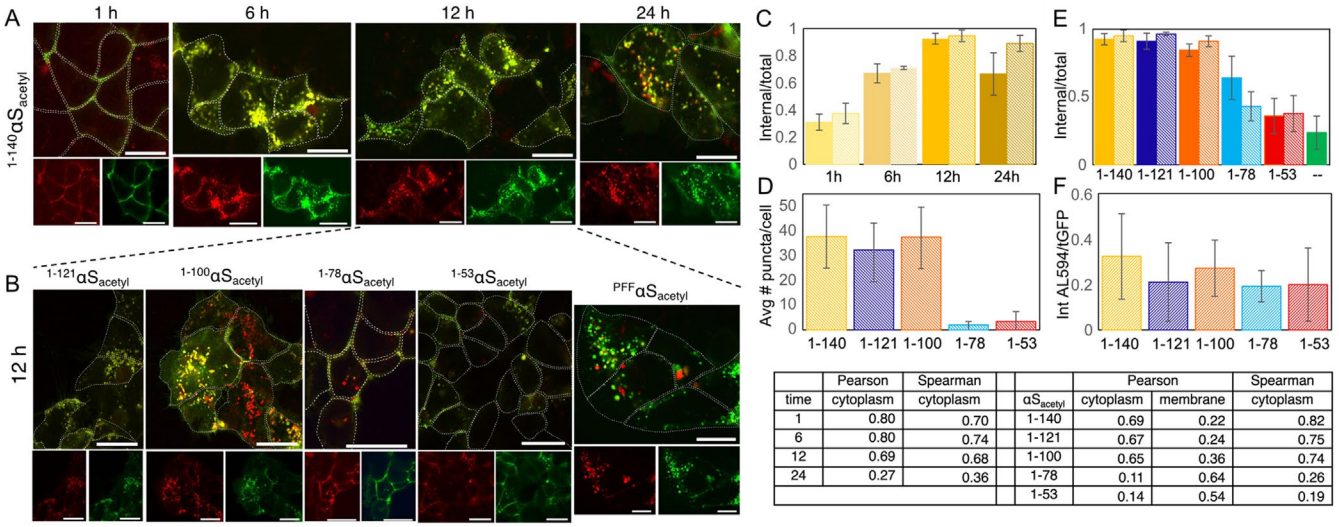

time	Pearson cytoplasm	Spearman cytoplasm
1	0.80	0.70
6	0.80	0.74
12	0.69	0.68
24	0.27	0.36

αS_{acetyl}	Pearson cytoplasm	Pearson membrane	Spearman cytoplasm
1-140	0.69	0.22	0.82
1-121	0.67	0.24	0.75
1-100	0.65	0.36	0.74
1-78	0.11	0.64	0.26
1-53	0.14	0.54	0.19

FIGURE 3: Internalization in HEK-N1β is reduced for truncated αS_{acetyl} constructs. (A) Representative images of HEK-N1β-tGFP cells following 1-h, 6-h, 12-h, and 24-h incubation with AL594 $^{1-140}\alpha S_{acetyl}$. The αS (red) and N1β (green) channels are shown separately below a larger image of their merge; cells are outlined in white dashed lines. (B) Representative images of HEK-N1β-tGFP cells following 12-h incubation with AL594 αS_{acetyl} truncations or $^{1-140}\alpha S_{acetyl}$ PFFs. The αS (red) and N1β (green) channels are shown separately below a larger image of their merge; cells are outlined in white dashed lines. (C) Internalization quantification for A) of N1β–tGFP (solid) and AL594 $^{1-140}\alpha S_{acetyl}$ (stripes) at the indicated incubation time. Colocalization was analyzed with the Pearson or Spearman correlation coefficient (Table). A larger coefficient reflects more overlap between the AL594 αS_{acetyl} and N1β–tGFP signals. Correlation coefficients were computed using the ImageJ plugin for colocalization. (D) Quantification of internalization for (B) of AL594 αS_{acetyl} truncations by HEK-N1β cells following 12-h incubation by puncta analysis. (E) Fraction of fluorescence signal of N1β-tGFP (solid) or AL594 αS_{acetyl} (stripes) from internalized proteins following 12-h incubation with AL594 αS_{acetyl} or control (–). (F) Quantification of binding of αS_{acetyl} constructs to HEK-N1β-tGFP treated with an endocytosis inhibitor to prevent internalization. (Table) Colocalization analysis of data from C) and E). Analysis for internalization and binding based on n = 100 cells, three independent experiments. Scale bars = 20 μm. Colocalization analysis based on *n* = 25 – 50 cells, three independent experiments.

Truncated αS_{acetyl} binds HEK-N1β

In contrast to SH-SY5Y cells, HEK293 cells do not spontaneously internalize $^{1-140}\alpha S_{acetyl}$ (Birol *et al.*, 2019). Expression of N1β in HEK293 cells, however, is sufficient to drive αS_{acetyl} uptake (Birol *et al.*, 2019). N1β with a C-terminal tGFP tag (N1β-tGFP) was expressed in HEK293 cells (HEK-N1β), where it localizes to the plasma membrane (Supplemental Figure S1). HEK-N1β were incubated 200 nM AL594 $^{1-140}\alpha S_{acetyl}$ for various amounts of time. Following 1-h incubation, both N1β and $^{1-140}\alpha S_{acetyl}$ can be visualized primarily on the plasma membrane (Figure 3A). By 6 h, there is significant internalization of both proteins, where they colocalize in intracellular puncta (Figure 3C). Colocalization of the intracellular proteins is observed at 12 h and 24 h, as well, although there is some slight separation of N1β and αS_{acetyl} at the 24-h timepoint suggesting that their processing pathways may be diverging (Figure 3, A and C). We observe a significant increase in the fraction of N1β signal on the cell membrane at 24 h (Supplemental Figure S2), while $^{1-140}\alpha S_{acetyl}$ remain as intracellular punctate structures (Figure 3, A and B); this may be the result of internalized N1β being trafficked back to the plasma membrane, or newly expressed N1β reaching the plasma membrane. Correlation analysis of these images confirms a decrease in the αS_{acetyl}/ N1β colocalization signal at 24 h (Figure 3, Table)

At 12-h incubation, internalized αS_{acetyl} and N1β-tGFP colocalize with LysoTracker Deep Red, which labels lysosomes and acidified endosomes (Supplemental Figure S3). In experiments with the addition of control buffer lacking αS_{acetyl}, the fraction of the cytoplasmic N1β is ~0.25 at 12 h (Figure 3E), comparable to what is observed in at 1 h (Supplemental Figure S2), indicating that there is no time-dependent behavior of the N1β signal in the absence of αS_{acetyl} treatment. We also created a construct of N1β bearing an N-terminal tGFP tag, tGFP-N1β; this tag precedes the signal sequence of N1β, and, as expected, when expressed in HEK293 cells, can be visualized throughout the cell body rather than localized to the plasma membrane (Supplemental Figure S1). HEK cells expressing tGFP-N1β do not spontaneously internalize $^{1-140}\alpha S_{acetyl}$ (Supplemental Figure S1), further underscoring the importance of the plasma membrane localization of N1β in driving uptake.

For comparison among the truncated αS_{acetyl} constructs, the 12-h incubation timepoint was chosen. As with the SH-SY5Y cells (Figure 2), when quantified by the fluorescence of intracellular puncta, internalization of $^{1-121}\alpha S_{acetyl}$ and $^{1-100}\alpha S_{acetyl}$ was comparable to that of $^{1-140}\alpha S_{acetyl}$ (Figure 3, B and D); neither $^{1-78}\alpha S_{acetyl}$ nor $^{1-53}\alpha S_{acetyl}$ showed significant internalization (Figure 3, B and D). Both $^{1-78}\alpha S_{acetyl}$ and $^{1-53}\alpha S_{acetyl}$ show evidence of plasma membrane localization, but many fewer internal puncta than the longer constructs (Figure 3D). Comparison of the fraction of internalized N1β and αS_{acetyl} following 12 h of incubation reveals that the majority the fluorescence signal originates from intracellular protein for the three longer αS_{acetyl} constructs, while significantly less of the fluorescence signal comes from intracellular protein for the two shorter αS_{acetyl} constructs (Figure 3E). At the same 12-h time-point, colocalization analysis of fluorescence from both N1β and αS_{acetyl} on the plasma membrane and in intracellular puncta show in inversion between the three longer and two shorter constructs (Figure 3, Table); for $^{1-140}\alpha S_{acetyl}$, $^{1-121}\alpha S_{acetyl}$, and $^{1-100}\alpha S_{acetyl}$ a large Pearson's coefficient for the internalized protein reflects a high degree of colocalization

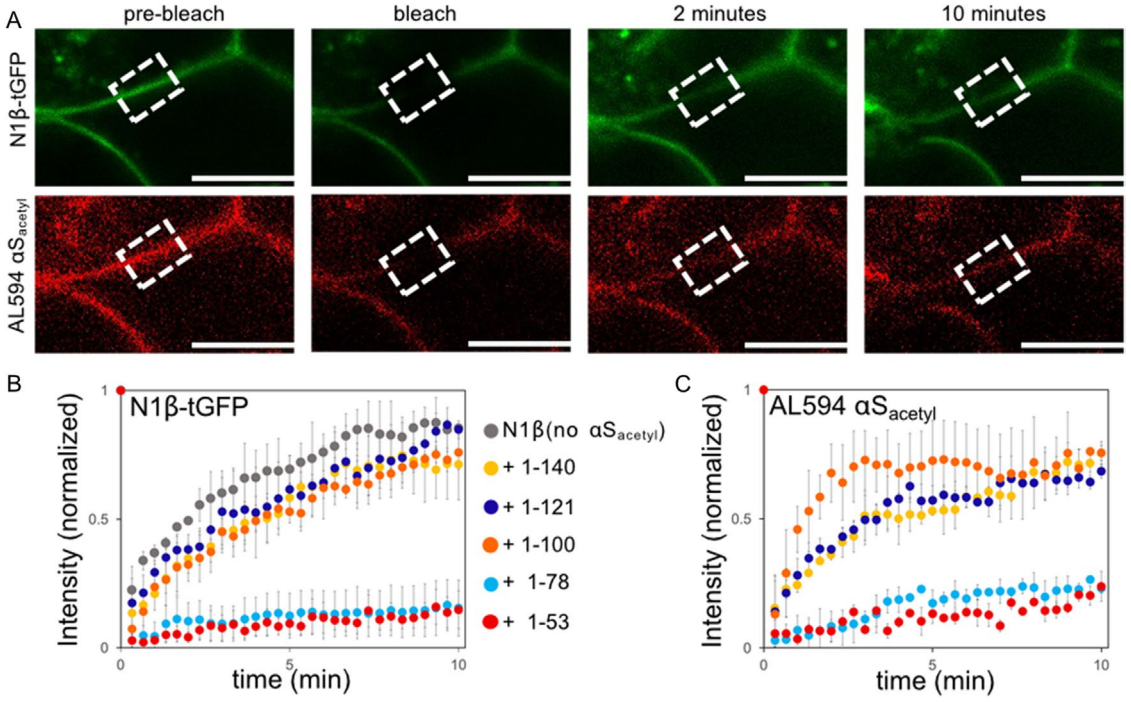

FIGURE 4: Internalization of αS_{acetyl} is correlated with dynamics on the cell membrane. (A) Representative images of HEK-N1β–tGFP with AL594 $^{1–140}\alpha S_{acetyl}$ bound used for FRAP analysis. (B) Averaged FRAP recovery curves of HEK-N1β and (C) AL594 αS_{acetyl} fluorescence, as labeled. Curves were corrected for steady-state photobleaching and normalized to control fluorescent levels. Two regions of interest from three independent experiments were chosen for FRAP. Scale bars = 10 μm.

with N1β, while a large Pearson's coefficient is calculated for plasma membrane localized $^{1–78}\alpha S_{acetyl}$ and $^{1–53}\alpha S_{acetyl}$. Conversely, the small Pearson's coefficients calculated for plasma-membrane localized $^{1–140}\alpha S_{acetyl}$, $^{1–121}\alpha S_{acetyl}$, and $^{1–100}\alpha S_{acetyl}$ and internalized $^{1–78}\alpha S_{acetyl}$ and $^{1–53}\alpha S_{acetyl}$ is due to the relatively small AL594 αS_{acetyl} signal as compared with that of N1β (Figure 3E). $^{1–90}\alpha S_{acetyl}$ uptake is comparable to the longer αS_{acetyl} constructs (Supplemental Figure S4), highlighting residues 79–90 as critical for differentiating internalization. Aggregated PFF $^{1–140}\alpha S_{acetyl}$ ($^{PFF}\alpha S_{acetyl}$) is internalized and colocalizes with N1β (Figure 3B). In the absence of N1β expression, none of the αS_{acetyl} constructs were spontaneously internalized by HEK293 cells (Supplemental Figure S5). Spearman's coefficients calculated for cytoplasmic proteins are consistent with the Pearson's analysis (Figure 3, Table)

We speculated that the observed differences in internalization between the constructs may be due to reduced binding of the shorter αS_{acetyl} constructs. To test this, we treated HEK-N1β cells with an endocytosis inhibitor (Dynasore hydrate) and took advantage of the fact that even in the absence of Dynasore, relatively little αS_{acetyl} is internalized by HEK-N1β at short timepoints (<1 h; Figure 3A). Each of the constructs was incubated with Dynasore-treated HEK-N1β cells for 30 min to allow for binding with minimal cellular uptake. Confocal imaging was used to quantify the relative signal of membrane-localized αS_{acetyl} normalized to the membrane-localized N1β signal, to account for cell-to-cell variability in N1β expression levels. Surprisingly, we found that all five constructs bind comparably at 200 nM (Figure 3F), indicating that differences in internalization of the various αS_{acetyl} constructs are not due to major differences in their affinities for HEK-N1β cells. The average expression levels of N1β, as measured by the signal intensity of the N1β channel in the binding experiments, is consistent across different imaging wells; thus differences in uptake are not due to significant differences in N1β expression between wells (Supplemental Figure S6). Importantly, our results demonstrate that while binding to N1β is localized to the N-terminal/NAC region of αS_{acetyl}, residues 79–90 are required for internalization. In prior work, the C-terminus of αS has been proposed to regulate interactions with membranes, other cellular receptors, as well as with itself (Crowther *et al.*, 1998; Bussell and Eliezer, 2001; Sevcsik *et al.*, 2011; Eliezer, 2013; Zhang *et al.*, 2021). Here, we demonstrate that residues 91–140 also regulate the interaction of αS_{acetyl} with N1β, enhancing N1β-mediated cellular uptake (Figures 2 and 3).

Truncation results in inhibited dynamics for N1β/plasma membrane associated αS_{acetyl}

To gain more insight into the nature of the interactions between αS_{acetyl} and N1β underlying uptake, fluorescence recovery after photobleaching (FRAP) was used to measure the dynamics both of AL594 αS_{acetyl} and N1β–tGFP in the plasma membrane of Dynasore-treated HEK-N1β cells (Figure 4A). In the absence of αS_{acetyl}, N1β fluorescence recovers on a timescale of ~3 min (Figure 4B). The fluorescence recovery of N1β following the addition of full-length $^{1–140}\alpha S_{acetyl}$, $^{1–121}\alpha S_{acetyl}$, or $^{1–100}\alpha S_{acetyl}$ does not change significantly (Figure 4C); moreover, when the fluorescence of the αS_{acetyl} was measured, the kinetics of the αS_{acetyl} fluorescence recovery tracks with that of N1β recovery for all three constructs.

In striking contrast, the fluorescence recovery of N1β in the presence of either $^{1–78}\alpha S_{acetyl}$ or $^{1–53}\alpha S_{acetyl}$ is dramatically slowed (Figure 4B); as with the other truncated constructs, $^{1–78}\alpha S_{acetyl}$ and $^{1–53}\alpha S_{acetyl}$ show similarly slowed dynamics (Figure 4C) relative to the longer constructs. Overall, the dynamics of diffusion of N1β appears to be correlated with the dynamics of the specific αS_{acetyl} construct; relatively rapid mobility on the cell surface seems essential for the efficient internalization of both proteins. The highly regulated

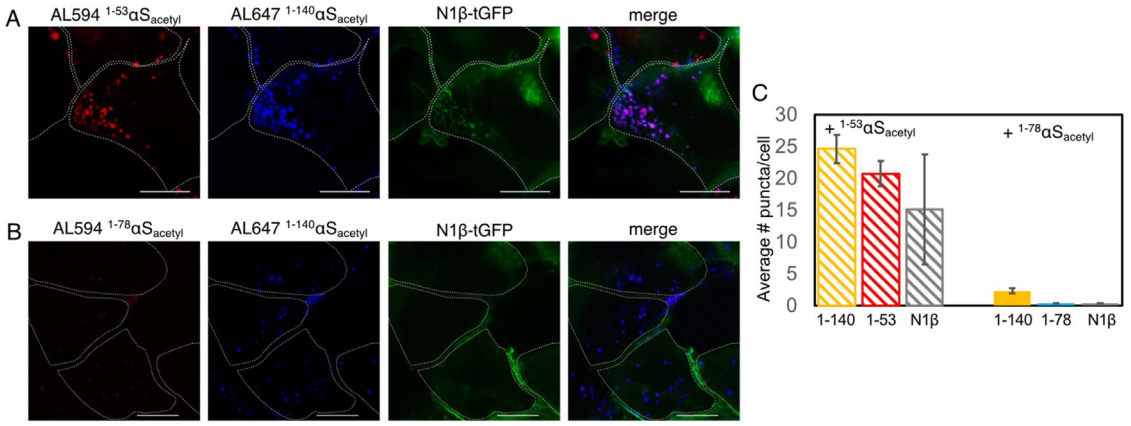

FIGURE 5: Internalization of $^{1–140}\alpha S_{acetyl}$ is diminished by $^{1–78}\alpha S_{acetyl}$. Representative images of HEK-N1β cells preincubated with AL594 $^{1–53}\alpha S_{acetyl}$ (A) or AL594 $^{1–78}\alpha S_{acetyl}$ (B). (C) Quantification of internalization of AL647 $^{1–140}\alpha S_{acetyl}$ from (A) and (B) by puncta analysis. Analysis based on n = 100 cells, two independent experiments. Scale bars = 20 μm.

surface mobility of N1β in neurons has been previously reported (Neupert *et al.*, 2015; Klatt *et al.*, 2021); changes in expression levels, membrane localization, and neuronal activity alter its diffusion. Moreover, N1β is cleaved by a number of extracellular proteases (Trotter *et al.*, 2019; Klatt *et al.*, 2021). It is possible that binding of some αS_{acetyl} constructs modifies this cleavage, impacting both N1β dynamics and αS_{acetyl}-mediated internalization. Here we identify binding of αS_{acetyl} as altering N1β dynamics, and consequently impacting intracellular trafficking of both proteins. Although molecular details of the inhibited diffusion and cellular uptake of the truncated αS_{acetyl} variants remain to be elucidated, our data provides direct evidence that the dynamic diffusion of N1β underlies αS_{acetyl} uptake.

Truncated αS_{acetyl} alters internalization of $^{1–140}\alpha S_{acetyl}$

Given their apparent ability to inhibit N1β dynamics, we were curious whether binding of the shorter, truncated variants inhibited internalization of full-length αS_{acetyl}. HEK-N1β cells were incubated with excess (1 μM total; 800 nM unlabeled protein and 200 nM AL594 labeled protein) $^{1–78}\alpha S_{acetyl}$ or $^{1–53}\alpha S_{acetyl}$ for 1 h to allow for binding; then 200 nM AL647 $^{1–140}\alpha S_{acetyl}$ was added and incubated for an additional 12 h. $^{1–140}\alpha S_{acetyl}$ was still internalized by HEK-N1β cells, even in the presence of five-fold excess of $^{1–53}\alpha S_{acetyl}$ (Figure 5A); in fact, under these conditions $^{1–140}\alpha S_{acetyl}$ drives internalization of $^{1–53}\alpha S_{acetyl}$, as seen by colocalization in cellular puncta of both αS_{acetyl} variants, along with N1β (Figure 5A). In contrast, $^{1–78}\alpha S_{acetyl}$ was effective at inhibiting uptake of $^{1–140}\alpha S_{acetyl}$ (Figure 5B). It appears that excess $^{1–78}\alpha S_{acetyl}$ likely blocks the binding site or regions on N1β critical to the internalization of full-length protein. By blocking uptake of $^{1–140}\alpha S_{acetyl}$, $^{1–78}\alpha S_{acetyl}$ also disrupts the uptake of N1β (Figure 5, B and C).

Through their interactions with binding partners in the postsynaptic membranes, neurexin family of proteins, including N1β, play a critical role in regulating the functional properties of synapses (Südhof, 2017), including formation and modification of synapses (Dean and Dresbach, 2006). Interestingly, a role for αS in synaptic plasticity has also been proposed, based on an early study showing a decrease in αS mRNA transcripts in regions of the zebra finch brain linked to song learning (George *et al.*, 1995). One study found that N1β interacted with αS PFFs (Mao *et al.*, 2016), with a subsequent paper suggesting the binding of αS PFFs could disrupt N1β-mediated synaptic organization (Feller *et al.*, 2023). Our own prior work demonstrated that the interaction between N1β and αS_{acetyl} monomer was chemically selective, dependent upon both the N-terminal acetylation of αS and the N-linked glycan on the extracellular domain of N1β (Birol *et al.*, 2019). Overall, this study contributes molecular insight in the interaction of these two proteins. Our findings highlight the importance of the C-terminus of αS_{acetyl} for mobility of N1β and αS_{acetyl} in the plasma membrane. In neurons, dynamic rearrangements on membranes are critical for synaptic transmission and plasticity. Our work suggests that dynamics of N1β may be regulated by binding of soluble protein ligands, including αS_{acetyl}. Interplay between N1β and monomer αS_{acetyl} may even be able to modify synaptic connectivity in neurons. Lastly, we demonstrate that a αS_{acetyl} truncation is capable of blocking binding to N1β by the full-length, physiological αS_{acetyl}, as well as inhibiting its subsequent internalization in cells, highlighting a potential approach for future therapeutic interventions.

MATERIALS AND METHODS

Request a protocol through *Bio-protocol*.

αS expression and purification

αS_{acetyl} was expressed in *E. coli* BL21 cells; BL21 stocks containing the N-terminal acetyltransferase B (NatB) plasmid with orthogonal antibiotic resistance were used. The NatB-BL21 cells were transformed with T7-7 plasmid containing the human αS sequence and grown in the presence of both chloramphenicol (34 μg/ml) and ampicillin (100 μg/ml) to select for both NatB and αS expression (as described in Birol *et al.*, 2019 with minor modifications). Briefly, two ammonium sulfate cuts were used (0.116 g/ml and 0.244 g/ml) with αS_{acetyl} precipitating in the second step. The pellet was resolubilized in Buffer A (25 mM Tris pH 8.0, 20 mM NaCl, 1 mM ethylenediaminetetraacetic acid [EDTA]) with 1 mM phenylmethylsulfonyl fluoride and dialyzed against Buffer A to remove ammonium sulfate. Dialyzed samples for $^{1–140}\alpha S_{acetyl}$ and $^{1–121}\alpha S_{acetyl}$ were loaded to an anion exchange column (GE HiTrap Q HP, 5 ml) and eluted with a gradient to 1 M NaCl. $^{1–140}\alpha S_{acetyl}$ elutes at ~300 mM NaCl. Fractions containing αS were pooled and concentrated using Amicon Ultra concentrators (3000 Da molecular weight cut-off). For $^{1–53}\alpha S_{acetyl}$, $^{1–78}\alpha S_{acetyl}$, $^{1–90}\alpha S_{acetyl}$, and $^{1–100}\alpha S_{acetyl}$, samples were loaded onto an anion exchange and flow-through was collected and concentrated. For all αS_{acetyl} constructs, concentrated samples were then loaded to a size exclusion column (GE HiLoad 16/600 Superdex75) and eluted at 0.5 ml/min. Fractions containing αS were again pooled and concentrated, then stored at –80°C. All αS constructs

used in this work were checked by matrix-assisted laser desorption/ionization (MALDI) to confirm correct mass and presence of acetylation.

αS labeling

For site-specific labeling of αS_{acetyl}, a cysteine was introduced at either residue nine or residue 130. For labeling reactions, freshly purified αS_{acetyl} (typically 200–300 µl of ~200 µM protein) was incubated with 1 mM dithiothreitol (DTT) for 30 min at room temperature to reduce the cysteine. The protein solution was passed over two coupled HiTrap Desalting Columns (GE Life Sciences, Pittsburgh, PA) to remove DTT and buffer exchanged into 20 mM Tris (pH 7.4), 50 mM NaCl, and 6 M guanidine hydrochloride (GdmCl). The protein was incubated overnight at 4°C with stirring with 4 × molar excess AL594 or AL647 maleimide (Invitrogen). The labeled protein was concentrated and buffer exchanged into 20 mM Tris pH 7.4, 50 mM NaCl using an Amicon Ultra 3K Concentrator (Millipore, Burlington, MA), with final removal of unreacted dye and remaining GdmCl by passing again over a set of coupled desalting columns equilibrated with 20 mM Tris pH 7.4, 50 mM NaCl.

Fibril formation

αS_{acetyl} PFFs were prepared as previously described (Volpicelli-Daley *et al.*, 2014). Briefly, 100 µM αS_{acetyl} was mixed with 5 µM AL594 αS_{acetyl} in 20 mM Tris pH 7.4, 100 mM NaCl. To induce aggregation, this solution was incubated at 37°C for 5 day with agitation (1500 rpm on an IKA MS3 digital orbital shaker) in parafilm-sealed 1.5 ml Eppendorf tubes to ensure minimal solvent evaporation. The aggregation reaction was analyzed by Congo Red absorbance by diluting 10 µl of the aggregation solution in 140 µl 20 µM Congo Red. The mature fibrils were then pelleted by centrifugation (13,200 rpm for 90 min at 4°C), and the supernatant was removed. Fibers were resuspended in an equal volume (relative to supernatant) of 20 mM Tris pH 7.4, 100 mM NaCl. Mature fibers were subsequently fragmented on ice using a sonicator (Diagenode UCD-300 bath sonicator) set to high, 30 s sonication followed by a delay period of 30 s – 10 min total – to form PFFs.

Cell culture

SH-SY5Y and HEK293 cells were grown at 37°C under a humidified atmosphere of 5% CO_2. The SH-SY5Y cells were cultured in Dulbecco's Modified Eagle's Medium (DMEM) plus 10% fetal bovine serum (FBS), 50 U/ml penicillin, and 50 µg/ml streptomycin. The HEK cells were cultured in DMEM supplemented with 10% FBS, 2 mM L-glutamine, and 100 U/ml each of penicillin and streptomycin. Cells were passaged upon reaching ~ 95% confluence (0.05% Trypsin-EDTA, Life Technologies, Carlsbad, CA), propagated, and/or used in experiments. Cells used in experiments were pelleted and resuspended in fresh media lacking Trypsin-EDTA.

For imaging of SH-SY5Y cells, cells were grown in eight-well Ibidi chambers (µ-Slide, eight-well glass bottom, Ibidi GmbH, Germany) which were coated with poly-D-lysine the night before. Chambers were seeded with 20,000–25,000 cells/well and cultured for 48 h before beginning experiments. For cellular uptake experiments, AL594-labeled αS_{acetyl} was added to cell media to a final concentration of 200 nM. Following incubation (0 to 24 h), the media were exchanged to remove noninternalized AL594 labeled αS_{acetyl} and cells were allowed to recovery briefly (30 min) before acquiring images.

Transfection of HEK cells

HEK cells were transfected with plasmid encoding the +SS4 isoform of N1β with a C-terminal tGFP tag (Origene; HEK-N1β) or N1β with an N-terminal tGFP tag (custom plasmid from Origene) by Lipofectamine 3000, following the manufacturer's directions. The HEK-N1β cells were grown to 70% confluency on eight-well ibidi chambers before transfection. Transfections were performed with 100 ng final concentration of N1β-tGFP or tGFP-N1β plasmid per 250 µl media per well. Transfection media was removed from cells 3 h later and fresh media was added. At 48 h following transfection, the media was exchanged with fresh media before the addition of αS. Cells were incubated with AL594 or AL647 αS_{acetyl} monomer (final concentration 200 nM) or PFFs (final concentration 200 nM monomer units, 1:20 labeled:unlabeled) for the indicated timepoints. Cells were then washed with fresh media before imaging.

For binding and FRAP experiments, cells were pretreated with the dynamin-dependent endocytosis blocker, Dynasore (Sigma-Aldrich, D7693), at 80 µM, 30 min before the addition of AL594 αS_{acetyl}.

Lysotracker

For colocalization of AL594 αS_{acetyl} and N1β-tGFP with lysosomes, cells were treated with 75 nM Lysotracker Deep Red (Life Technologies, Carlsbad, CA) for 1 h before imaging.

Internalization blocking experiments

HEK-N1β cells were incubated with 1 µM (800 nM dark and 200 nM AL594 labeled) $^{1–53}\alpha S_{acetyl}$ or $^{1–78}\alpha S_{acetyl}$ for 1 h, followed by addition of 200 nM AL647 $^{1–140}\alpha S_{acetyl}$. The cells were incubated for another 12 h and then washed with media before imaging.

Cell imaging and analysis

All cell imaging was carried out by confocal fluorescence microscopy using an Olympus FV3000 scanning system configured on a IX83 inverted microscope platform with a 60 × Plan-Apo/1.1-NA water-immersion objective with DIC capability (Olympus, Tokyo, Japan). For all experiments, the gain setting for the channels was kept constant from sample to sample: for detection of N1β-tGFP, blue channel excitation 488 nm, emission BP 500–540 nm, for detection of AL594 αS_{acetyl}, green channel excitation 561 nm, emission BP 570–620 nm and for detection of AL647 αS_{acetyl} or LysoTracker Deep Red, red channel excitation 640 nm, emission BP 660–720 nm.

Most image acquisition and processing were performed with the software accompanying the FV3000 microscope and Image J software (Schneider *et al.*, 2012). For SH-SY5Y cells, internalized αS_{acetyl} was quantified either by analysis of the punctate structures in the cells or by the total cellular fluorescence. For total cellular fluorescence, the integrated fluorescence intensity of the cells is reported. Cellular puncta were analyzed using the ImageJ particle analysis plug-in. This algorithm detects puncta through a user-defined threshold and counts the number of puncta that meet or exceed the threshold. The threshold was initially defined by manual identification and averaging of a subset of puncta. Colocalization with N1β was computed by obtaining a Pearson or Spearman coefficient using the ImageJ plugin for colocalization (Coloc_2). The total intensity of AL594 αS_{acetyl} and N1β-tGFP on the cell membrane and inside the cell was quantified by masking the cell membrane and then defining the inside of the masked area as the cell interior. The ImageJ "measure" command was used to get the average intensity integrated over each masked area (cell membrane) and the cell interior separately. Colocalization analysis was carried out on 5–10 frames of cell images, each frame containing at least five cells for a total of 25–50 cells.

For some of the experiments, imaging was carried out on a PicoQuant MicroTime 200 time-resolved fluorescence system based on an inverted Olympus IX73 microscope (Olympus, Tokyo, Japan). A 60X Plan-Apo/1.4-NA water-immersion objective, 482 and 560 nm excitation lasers and a frame size of 512 × 512 pixels was used. Images acquired with this instrument were in lifetime mode but were integrated to obtain intensity-based images comparable to typical confocal images. Fluorescence intensities were analyzed via the lifetime mode using SymPhoTime 64 (PicoQuant, Berlin, Germany). The intensity of images was then adjusted on ImageJ analysis program.

FRAP

FRAP was performed on the same Olympus confocal microscope described above. A 128 × 128 pixel image was captured at 0.188 s intervals using the 488 nm and 561 nm laser lines at 1% power and the pinhole set to 105 µm. Following 20 prebleach frames, a 50 × 50 pixel region was bleached at full power for 0.94 s (one scan iteration). Images were captured until no further recovery was evident. Image stacks were loaded, and both the rough center of the bleach area and an appropriate unbleached reference area were selected manually. Mean fluorescence was monitored within the bleached region as well as within the manually specified reference region to control for photobleaching. Individual recovery curves were normalized to the reference curves, and then to prebleach values.

ACKNOWLEDGMENTS

We thank T. Baumgart for use of his confocal microscope and V. M.-Y. Lee for use of her sonicator. This work was supported by the University of Pennsylvania and the National Institutes of Health (R01 NS-120625 to E.R.) and MDC-Berlin (I.I.D.M.).

REFERENCES

Anderson JP, Walker DE, Goldstein JM, de Laat R, Banducci K, Caccavello RJ, Barbour R, Huang J, Kling K, Lee M, *et al.* (2006). Phosphorylation of Ser-129 is the dominant pathological modification of alpha-synuclein in familial and sporadic Lewy body disease. J Biol Chem 281, 29739–29752.

Bendor JT, Logan TP, Edwards RH (2013). The function of α-synuclein. Neuron 79, 1044–1066.

Beyer K (2006). Alpha-synuclein structure, posttranslational modification and alternative splicing as aggregation enhancers. Acta Neuropathol 112, 237–251.

Beyer K, Ariza A (2013). α-Synuclein posttranslational modification and alternative splicing as a trigger for neurodegeneration. Mol Neurobiol 47, 509–524.

Bhattacharjee P, Öhrfelt A, Lashley T, Blennow K, Brinkmalm A, Zetterberg H (2019). Mass spectrometric analysis of Lewy body-enriched α-Synuclein in Parkinson's disease. J Proteome Res 18, 2109–2120.

Bieri G, Gitler AD, Brahic M (2018). Internalization, axonal transport and release of fibrillar forms of alpha-synuclein. Neurobiol Dis 109, 219–225.

Birol M, Wojcik SP, Miranker AD, Rhoades E (2019). Identification of N-linked glycans as specific mediators of neuronal uptake of acetylated α-Synuclein. PLoS Biol 17, e3000318.

Bussell R, Jr., Eliezer D (2001). Residual structure and dynamics in Parkinson's disease-associated mutants of alpha-synuclein. J Biol Chem 276, 45996–46003.

Bussell R, Jr., Eliezer D (2003). A structural and functional role for 11-mer repeats in alpha-synuclein and other exchangeable lipid binding proteins. J Mol Biol 329, 763–778.

Crowther RA, Jakes R, Spillantini MG, Goedert M (1998). Synthetic filaments assembled from C-terminally truncated alpha-synuclein. FEBS Lett 436, 309–312.

Davidson WS, Jonas A, Clayton DF, George JM (1998). Stabilization of alpha-synuclein secondary structure upon binding to synthetic membranes. J Biol Chem 273, 9443–9449.

Dean C, Dresbach T (2006). Neuroligins and neurexins: linking cell adhesion, synapse formation and cognitive function. Trends Neurosci 29, 21–29.

Diaz-Ortiz ME, Seo Y, Posavi M, Carceles Cordon M, Clark E, Jain N, Charan R, Gallagher MD, Unger TL, Amari N, *et al.* (2022). GPNMB confers risk for Parkinson's disease through interaction with α-synuclein. Science 377, eabk0637.

Eliezer D (2013). The mysterious C-terminal tail of alpha-synuclein: nanobody's guess. J Mol Biol 425, 2393–2396.

Emmanouilidou E, Melachroinou K, Roumeliotis T, Garbis SD, Ntzouni M, Margaritis LH, Stefanis L, Vekrellis K (2010). Cell-produced alpha-synuclein is secreted in a calcium-dependent manner by exosomes and impacts neuronal survival. J Neurosci 30, 6838–6851.

Feller B, Fallon A, Luo W, Nguyen PT, Shlaifer I, Lee AK, Chofflet N, Yi N, Khaled H, Karkout S, *et al.* (2023). α-Synuclein preformed fibrils bind to β-neurexins and impair β-neurexin-mediated presynaptic organization. Cells 12, 1083.

Ferreon AC, Gambin Y, Lemke EA, Deniz AA (2009). Interplay of alpha-synuclein binding and conformational switching probed by single-molecule fluorescence. Proc Natl Acad Sci USA 106, 5645–5650.

Fortin DL, Troyer MD, Nakamura K, Kubo S, Anthony MD, Edwards RH (2004). Lipid rafts mediate the synaptic localization of alpha-synuclein. J Neurosci 24, 6715–6723.

Galvin JE, Uryu K, Lee VM, Trojanowski JQ (1999). Axon pathology in Parkinson's disease and Lewy body dementia hippocampus contains alpha-, beta-, and gamma-synuclein. Proc Natl Acad Sci USA 96, 13450–13455.

George JM, Jin H, Woods WS, Clayton DF (1995). Characterization of a novel protein regulated during the critical period for song learning in the zebra finch. Neuron 15, 361–372.

Guerrero-Ferreira R, Taylor NM, Mona D, Ringler P, Lauer ME, Riek R, Britschgi M, Stahlberg H (2018). Cryo-EM structure of alpha-synuclein fibrils. eLife 7, e36402.

Guo JL, Lee VM (2014). Cell-to-cell transmission of pathogenic proteins in neurodegenerative diseases. Nat Med 20, 130–138.

Jao CC, Der-Sarkissian A, Chen J, Langen R (2004). Structure of membrane-bound alpha-synuclein studied by site-directed spin labeling. Proc Natl Acad Sci U S A 101, 8331–8336.

Johnson M, Coulton AT, Geeves MA, Mulvihill DP (2010). Targeted amino-terminal acetylation of recombinant proteins in E. coli. PLoS One 5, e15801.

Kahle PJ, Neumann M, Ozmen L, Muller V, Jacobsen H, Schindzielorz A, Okochi M, Leimer U, van Der Putten H, Probst A, *et al.* (2000). Subcellular localization of wild-type and Parkinson's disease-associated mutant alpha -synuclein in human and transgenic mouse brain. J Neurosci 20, 6365–6373.

Kang JH, Mollenhauer B, Coffey CS, Toledo JB, Weintraub D, Galasko DR, Irwin DJ, Van Deerlin V, Chen-Plotkin AS, Caspell-Garcia C, *et al.* (2016). CSF biomarkers associated with disease heterogeneity in early Parkinson's disease: the Parkinson's Progression Markers Initiative study. Acta Neuropathol 131, 935–949.

Kellie JF, Higgs RE, Ryder JW, Major A, Beach TG, Adler CH, Merchant K, Knierman MD (2014). Quantitative measurement of intact alpha-synuclein proteoforms from post-mortem control and Parkinson's disease brain tissue by intact protein mass spectrometry. Sci Rep 4, 5797.

Klatt O, Repetto D, Brockhaus J, Reissner C, El Khallouqi A, Rohlmann A, Heine M, Missler M (2021). Endogenous β-neurexins on axons and within synapses show regulated dynamic behavior. Cell Rep 35, 109266.

Krishna A, Biryukov M, Trefois C, Antony PM, Hussong R, Lin J, Heinäniemi M, Glusman G, Köglsberger S, Boyd O, *et al.* (2014). Systems genomics evaluation of the SH-SY5Y neuroblastoma cell line as a model for Parkinson's disease. BMC Genomics 15, 1154.

Lee HJ, Patel S, Lee SJ (2005). Intravesicular localization and exocytosis of alpha-synuclein and its aggregates. J Neurosci 25, 6016–6024.

Li B, Ge P, Murray KA, Sheth P, Zhang M, Nair G, Sawaya MR, Shin WS, Boyer DR, Ye S, *et al.* (2018). Cryo-EM of full-length α-synuclein reveals fibril polymorphs with a common structural kernel. Nat Commun 9, 3609.

Mao X, Ou MT, Karuppagounder SS, Kam TI, Yin X, Xiong Y, Ge P, Umanah GE, Brahmachari S, Shin JH, *et al.* (2016). Pathological α-synuclein transmission initiated by binding lymphocyte-activation gene 3. Science 353, aah3374.

Maroteaux L, Campanelli JT, Scheller RH (1988). Synuclein: a neuron-specific protein localized to the nucleus and presynaptic nerve terminal. J Neurosci 8, 2804–2815.

Middleton ER, Rhoades E (2010). Effects of curvature and composition on α-synuclein binding to lipid vesicles. Biophys J 99, 2279–2288.

Nath A, Sammalkorpi M, DeWitt DC, Trexler AJ, Elbaum-Garfinkle S, O'Hern CS, Rhoades E (2012). The conformational ensembles of α-synuclein and tau: combining single-molecule FRET and simulations. Biophys J 103, 1940–1949.

Neupert C, Schneider R, Klatt O, Reissner C, Repetto D, Biermann B, Niesmann K, Missler M, Heine M (2015). Regulated dynamic trafficking of neurexins inside and outside of synaptic terminals. J Neurosci 35, 13629–13647.
Rodriguez L, Marano MM, Tandon A (2018). Import and export of misfolded α-Synuclein. Front Neurosci 12, 344.
Schneider CA, Rasband WS, Eliceiri KW (2012). NIH Image to Image J: 25 years of image analysis. Nat Methods 9, 671–675.
Sevcsik E, Trexler AJ, Dunn JM, Rhoades E (2011). Allostery in a disordered protein: oxidative modifications to α-synuclein act distally to regulate membrane binding. J Am Chem Soc 133, 7152–7158.
Shrivastava AN, Redeker V, Fritz N, Pieri L, Almeida LG, Spolidoro M, Liebmann T, Bousset L, Renner M, Léna C, *et al.* (2015). α-synuclein assemblies sequester neuronal α3-Na+/K+-ATPase and impair Na+ gradient. EMBO J 34, 2408–2423.
Spillantini MG, Crowther RA, Jakes R, Hasegawa M, Goedert M (1998). alpha-Synuclein in filamentous inclusions of Lewy bodies from Parkinson's disease and dementia with lewy bodies. Proc Natl Acad Sci U S A 95, 6469–6473.
Südhof TC (2017). Synaptic neurexin complexes: a molecular code for the logic of neural circuits. Cell 171, 745–769.
Theillet FX, Binolfi A, Bekei B, Martorana A, Rose HM, Stuiver M, Verzini S, Lorenz D, van Rossum M, Goldfarb D, Selenko P (2016). Structural disorder of monomeric α-synuclein persists in mammalian cells. Nature 530, 45–50.
Trexler AJ, Rhoades E (2009). Alpha-synuclein binds large unilamellar vesicles as an extended helix. Biochemistry 48, 2304–2306.
Trexler AJ, Rhoades E (2010). Single molecule characterization of α-synuclein in aggregation-prone states. Biophys J 99, 3048–3055.
Trexler AJ, Rhoades E (2012). N-Terminal acetylation is critical for forming α-helical oligomer of α-synuclein. Protein Sci 21, 601–605.
Trotter JH, Hao J, Maxeiner S, Tsetsenis T, Liu Z, Zhuang X, Südhof TC (2019). Synaptic neurexin-1 assembles into dynamically regulated active zone nanoclusters. J Cell Biol 218, 2677–2698.
Tuttle MD, Comellas G, Nieuwkoop AJ, Covell DJ, Berthold DA, Kloepper KD, Courtney JM, Kim JK, Barclay AM, Kendall A, *et al.* (2016). Solid-state NMR structure of a pathogenic fibril of full-length human α-synuclein. Nat Struct Mol Biol 23, 409–415.
Urrea L, Ferrer I, Gavín R, Del Río JA (2017). The cellular prion protein (PrP(C)) as neuronal receptor for α-synuclein. Prion 11, 226–233.
van Steenoven I, Majbour NK, Vaikath NN, Berendse HW, van der Flier WM, van de Berg WDJ, Teunissen CE, Lemstra AW, El-Agnaf OMA (2018). α-Synuclein species as potential cerebrospinal fluid biomarkers for dementia with Lewy bodies. Mov Disord 33, 1724–1733.
Volpicelli-Daley LA, Luk KC, Lee VM (2014). Addition of exogenous α-synuclein preformed fibrils to primary neuronal cultures to seed recruitment of endogenous α-synuclein to Lewy body and Lewy neurite-like aggregates. Nat Protoc 9, 2135–2146.
Yamada K, Iwatsubo T (2018). Extracellular α-synuclein levels are regulated by neuronal activity. Mol Neurodegener 13, 9.
Zambon F, Cherubini M, Fernandes HJR, Lang C, Ryan BJ, Volpato V, Bengoa-Vergniory N, Vingill S, Attar M, Booth HDE, *et al.* (2019). Cellular α-synuclein pathology is associated with bioenergetic dysfunction in Parkinson's iPSC-derived dopamine neurons. Hum Mol Genet 28, 2001–2013.
Zhang S, Liu YQ, Jia C, Lim YJ, Feng G, Xu E, Long H, Kimura Y, Tao Y, Zhao C, *et al.* (2021). Mechanistic basis for receptor-mediated pathological α-synuclein fibril cell-to-cell transmission in Parkinson's disease. Proc Natl Acad Sci U S A 118, e2011196118.